Spin-polarized 129Xe NMR study of a polymer surface

ARTICLE *in* THE JOURNAL OF PHYSICAL CHEMISTRY · FEBRUARY 1993

Impact Factor: 2.78 · DOI: 10.1021/j100110a029

Spin-Polarized ^{129}Xe NMR Study of a Polymer Surface

D. Raftery,† L. Reven,‡ H. Long, and A. Pines*

Materials Sciences Division, Lawrence Berkeley Laboratory, and Department of Chemistry, University of California, Berkeley, California 94720

P. Tang and J. A. Reimer

Center for Advanced Materials, Lawrence Berkeley Laboratory, and Department of Chemical Engineering, University of California, Berkeley, California 94720

Received: August 14, 1992; In Final Form: November 5, 1992

A method for NMR studies of low surface area materials using optically pumped xenon gas is described. The method has been used to investigate spin-polarized xenon adsorbed onto poly(acrylic acid). The temperature dependence of the xenon–surface interaction, as measured by the xenon chemical shifts extrapolated to zero pressure, is shown to be consistent with a simple model of chemical exchange between the gas and adsorbed phases. The magnitude of the surface contribution to the ^{129}Xe chemical shift indicates a relatively strong interaction between xenon and poly(acrylic acid), possibly due to the polar carboxylic acid functional groups at the polymer surface. From the pressure dependence of the ^{129}Xe shift, the diffusion coefficient of xenon on poly(acrylic acid) is estimated to be 3.3×10^{-5} cm^2/s.

I. Introduction

The surface and interfacial characteristics of solid systems, such as inorganic solids, polymers, and thin films, are important to many of their useful material properties. The task of relating the microscopic structure to their macroscopic physical properties, however, has been hindered by the lack of suitable techniques capable of probing these materials. Due to their instability under ultrahigh-vacuum conditions, organic solids and catalytic materials such as metal oxides are difficult to study by the surface science techniques that have been successfully employed for single-crystal studies. As a nonintrusive experimental method capable of giving dynamic and structural information at an atomic level, nuclear magnetic resonance spectroscopy should be an attractive probe of heterogeneous surfaces. Indeed, through the development of high-resolution techniques, NMR has contributed greatly toward the chemical and physical understanding of bulk solids.[1] The main obstacle to the successful application of NMR to surface studies is, of course, its low sensitivity compared to other spectroscopic methods as well as the problem of distinguishing between the surface and bulk spins.

Various approaches to increasing the NMR signal have been pursued, such as isotopic enrichment, high applied magnetic fields, millikelvin NMR,[2] and cross polarization.[3] These experiments, which are based on increasing the equilibrium magnetization, do not, in general, give the signal enhancements required to detect the surface spins of materials with surface areas lower than ~10 m^2/g. Another approach toward enhancing the magnetic resonance signal is to produce a large nonequilibrium magnetization by optical pumping.[4] Large nuclear spin polarization of xenon and other noble gases can be created via spin exchange collisions with optically pumped alkali metal vapor. These experiments have long been employed to measure fundamental physical quantities and to study spin relaxation processes in the gas phase.[5] Due to the formation of relatively long lived van der Waals molecules, xenon can be efficiently spin polarized through collisions with optically pumped rubidium vapor,[6] allowing the investigation of surface interactions between ^{131}Xe gas and glass cell walls.[7] More recently, the spin–lattice relaxation of solid ^{129}Xe has been measured by transfer of frozen optically pumped xenon to a magnet.[8]

Concurrently, conventional ^{129}Xe NMR has become a widely employed technique for the characterization of porous solids. In particular, xenon NMR has been used to elucidate the structures of zeolites[9] and to detect dispersed metal particles[10] and adsorbed guest molecules[11] within the zeolite cages. Occluded xenon has also been used to investigate clathrates,[12] pillared clays,[13] semicrystalline polymers,[14] and proteins.[15] Xenon is an excellent NMR probe of these internal surfaces due to its large polarizable electron cloud, which gives rise to a very large chemical shift range that is extremely sensitive to the surrounding microscopic environment. The main limitation of ^{129}Xe NMR, is that, unless the temperature is very low,[2] and the T_1 is short, the sensitivity is unfavorable and one is often limited to systems of very high surface areas.[16,17]

We recently demonstrated[18] that by combining optical pumping of xenon gas with high-field NMR the ^{129}Xe NMR signal of xenon adsorbed onto materials with low-to-moderate surface areas may be readily observed. Optical pumping provides an enhancement of the ^{129}Xe NMR signal by more than three orders of magnitude which extends xenon NMR to nonporous solids with much lower surface areas. Since ordinary, nonporous solids with particle sizes on the order of 10 microns have surface areas around 1–10 m^2/g, adsorption studies on a wide range of materials are possible with this experiment.

In this paper, we describe in detail the experimental apparatus and procedure that were introduced in our preliminary reports on high field NMR of optically pumped xenon.[18,19] Results of our investigations of spin-polarized xenon adsorbed on powdered poly(acrylic acid) are presented. Amorphous poly(acrylic acid) has a moderate surface area (~15 m^2/g), and xenon was found to have both a relatively long relaxation time and significant surface interaction on this polymer. The chemical shift of adsorbed xenon as a function of temperature and pressure is shown to yield information about the xenon–surface interaction and the diffusion of xenon over the polymer surface. A simple model is developed for the magnitude of the xenon–surface interaction as measured by the temperature dependence of the chemical shift extrapolated to zero xenon pressure. From the pressure depen-

† Present address: Department of Chemistry, University of Pennsylvania, Philadelphia, PA 19104.

‡ Present address: Department of Chemistry, McGill University, Montreal, PQ Canada H3A2K6.

0022-3654/93/2097-1649$04.00/0

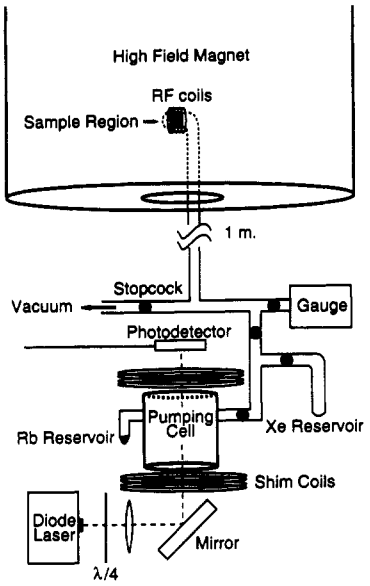

Figure 1. Schematic diagram of the experimental apparatus. Circularly polarized 794.7-nm laser light is focused onto the optical pumping cell. A silicon photodetector is used to detect the rubidium absorption. The oven used to heat the pumping cell and the nitrogen cooling system for the sample region are not shown. Shim coils can be used to cancel gradients and/or reduce the overall magnetic field in the pumping cell.

dence of the chemical shift, a rough estimate is made of the diffusion coefficient of xenon at monolayer coverages on poly(acrylic acid).

II. Experimental Methods

Apparatus. The apparatus, shown schematically in Figure 1, consists of an optical pumping cell located in the fringe magnetic field (250 G) underneath a 4.4-T superconducting magnet and a sample cell located in high field. The two regions are connected by some glassware and are separated by a series of stopcocks. A connection to a vacuum rack allows for evacuation of the sample region and a connecting tube to gauges for pressure measurements during the experiment. Natural-abundance rubidium is contained in a sidearm connected to a pumping cell heated with a flow of nitrogen gas. The rubidium is optically pumped to a polarization level approaching 100% using circularly polarized light from a temperature-stabilized, 40-mW, single-mode semiconductor diode laser (Model LT016, Sharp Electronics Corp., Mahwah, NJ) operating at the 794.7 nm rubidium D1 transition. The diode laser is temperature tuned and controlled to within ±0.01 K using two layers of thermoelectric cooler elements and temperature controllers (Light Wave Co., Bozeman, MT). The diode laser, which is located in a nitrogen filled vacuum enclosure, illuminates approximately two-thirds of the cell volume. The entire glass manifold is coated with Surfrasil (Pierce Chemical Co. Rockford, IL) a siliconizing agent that increases the wall-induced relaxation time of ^{129}Xe to greater than 30 min. The cylindrical optical pumping cell of approximately 11 cm^3 volume is filled with between 100 and 600 Torr of enriched (80%) xenon-129. A Helmholtz pair of shim coils is used in the low-pressure experiments to reduce the fringe magnetic field to approximately 50 G, which has the effect of increasing the spin-exchange efficiency at low pressures.[20]

NMR Probe. A schematic drawing of the sample region of the NMR probe used in these experiments is shown in Figure 2. The main features of the probe are a Macor ceramic coil support, glass dewar, dewared stainless steel transfer line for the nitrogen cooling gas, and a glass transfer line for the polarized xenon. The temperature range with this design extends down to −170 °C and controls the temperature to within ±1 °C. Since at very cold temperatures the xenon has a tendency to freeze out onto the

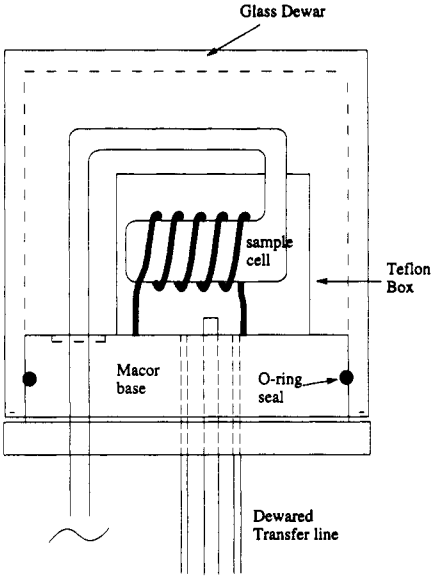

Figure 2. Drawing of the sample region of the probe used for xenon optical pumping experiments in high field.

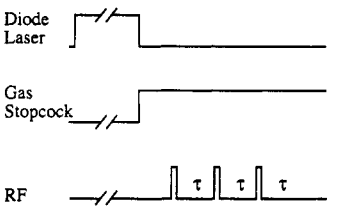

Figure 3. Timing diagram for data acquisition.

glass tubing walls before reaching the sample, a Teflon enclosure was constructed about the rf coil to limit the coldest part of the dewared region to the immediate sample region. An rf-shielded thermocouple is inserted into the Teflon container to monitor and control the temperature at the sample. The double-resonance rf circuit, based on a design by Doty and co-workers,[21] has the advantage of good efficiency at the xenon resonance frequency at 51.4 MHz while allowing for a large sample volume of about 8 cm^3.

Experimental Procedure. The timing diagram for the experiment is shown in Figure 3. The rubidium vapor, with xenon gas added, is optically pumped for approximately 30 min at temperatures between 80 and 120 °C, so that the adsorption of incident pumping light is between 50% and 100%. After pumping, the cell is cooled to approximately 40 °C to reduce the vapor pressure of rubidium in the pumping cell. The spin-polarized xenon does not relax appreciably during this cooling period (~1 min). The stopcock is then opened and polarized xenon flows (in less than 1 s) up to the sample region where it can adsorb onto the sample. To allow the xenon to reach equilibrium after adsorption onto the sample, we typically wait 30–60 s before acquiring data. Spectra are recorded by Fourier transformation of the signal following a short (typically 45°) rf pulse at 51.4 MHz. The NMR signal is typically obtained in a single scan with sufficient signal-to-noise ratio.

The equilibration of xenon with the surface was checked in separate experiments by applying small tipping angle pulses at 10-s intervals and observing the time-independent spectra after several scans. This also allows us to estimate the relaxation time of ~30 s. The xenon equilibration was independently checked with a sealed sample of treated (see below) poly(acrylic acid) filled with ~3 atm of enriched (80%) xenon-129 and ~100 Torr of oxygen to reduce the T_1 to <5 s. This sample was slowly cooled and brought to thermal equilibration at several temperatures that were used in the optical pumping experiments. The spectra showed line widths identical with optical pumping spectra

on the treated polymer. We have shown with several samples (e.g., zeolites, carbon black) that when xenon does not reach equilibrium with a surface the line width is time dependent and larger than when it is in equilibrium.[18]

With the pumping cell in the 250 G fringe field of the magnet, we obtained spectra for optically pumped xenon gas typically with signal-to-noise enhancements of about 800 over a conventional high-field NMR spectrum. However, after lowering the fringe field down to 50 G with the Helmholtz coils and reducing the gas pressure to less than 100 Torr, the signal-to-noise enhancement was increased to about 2000. Conventional experiments with signal averaging one shot every T_1 for our pumping period would realize an increase in signal-to-noise of only ~8 and thus would be unable to observe the adsorbed xenon under the conditions of this experiment. Adding oxygen as we did in our sealed sample mentioned above would increase the rate of signal accumulation; however, it would introduce a contact shift that would be difficult to assess on a surface.

After the data acquisition, the sample is allowed to warm and the xenon is recycled by freezing it back into the xenon reservoir (see Figure 1) with liquid nitrogen. Since the xenon sometimes becomes slightly contaminated during the experiment, the xenon is purified before being returned to the pumping cell by first heating it with a small amount of rubidium metal in the xenon reservoir. Water and other contaminants react very quickly with the rubidium vapor. The xenon must be very pure since the rubidium concentration in the pumping cell is only ~10^{-5} Torr and a very small amount of contaminant will greatly diminish the pumping efficiency.

Sample Treatment. The preparation of a clean surface is a main concern in surface studies. Although with powdered or organic materials it is impossible to use the pretreatments employed in conventional surface science techniques (annealing, polishing or sputtering), we did try to treat our samples in a manner consistent with other studies of powdered materials. This consisted of evacuation at room temperature or higher to eliminate as much as possible, physisorbed molecules such as water or oxygen. Powdered poly(acrylic acid) (Aldrich, Milwaukee, WI) was treated overnight under vacuum at 80 °C since water adsorbs strongly on this polymer. As discussed below, the surface treatment strongly affected the NMR spectra of xenon adsorbed on poly(acrylic acid). The sample was then loaded into the probe in a N_2 filled glovebag and then immediately evacuated to below 10^{-5} Torr and stored under vacuum until the xenon gas was introduced.

Isotherms. Nitrogen and xenon isotherms were carried out to measure the surface area and adsorption energy of xenon on poly(acrylic acid), and the BET isotherm[22] gave an excellent fit to the data. The equation for a BET isotherm is

$$V = \frac{V_{mon}cx}{(1-x)[1+x(c-1)]} \quad (1)$$

where V is the volume of adsorbed gas at STP, $x = p/p_0$ is the reduced pressure, and V_{mon} is the volume that would be occupied at STP by the amount of gas needed to form a monolayer on 1 g of sample. The quantity c is related to the surface adsorption energy by the relation

$$\ln c = (\Delta H_{ads} - \Delta H_l)/RT \quad (2)$$

where ΔH_l is the heat of liquefaction of the adsorbate. Isotherm data were collected on a glass vacuum rack using a silicone oil diffusion pump capable of pressures below 10^{-5} Torr. For the xenon isotherms conducted at low temperatures, cold-temperature baths such as liquid nitrogen/acetone were used. For accuracy, the dead-volume measurements using helium gas were made at each temperature an isotherm was carried out. A final temperature correction to STP was made once V_{mon} was calculated.

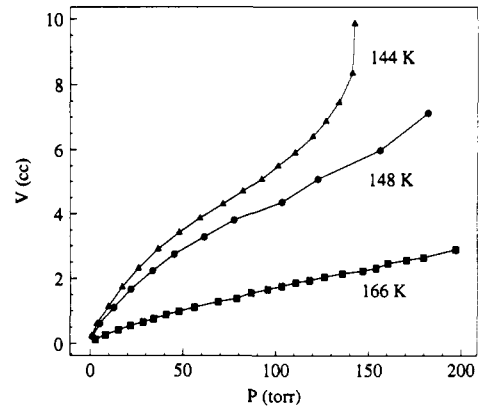

Figure 4. BET isotherms of xenon on poly(acrylic acid) at 144, 148, and 166 K. Lines connect the points to guide the eye.

TABLE I: Summary of the Isotherm Data for Nitrogen and Xenon Adsorbed onto Poly(acrylic acid)

gas	temp (K)	ΔH_{ads} (kcal/mol)	area (m^2/g)
xenon	166	4.22	17.2
xenon	148	4.23	16.7
xenon	144	4.21	15.7
nitrogen	77	2.28	14.4

As seen in Figure 4, the xenon isotherms on poly(acrylic acid) at 144, 148, and 166 K show characteristic BET behavior. The parameters for the xenon and nitrogen isotherms are listed in Table I. Although the surface areas derived from the xenon isotherms are slightly larger than those from the nitrogen surface area measurement, the adsorption energies for xenon are relatively constant. To use the isotherm parameters to analyze our chemical shift data for ^{129}Xe on poly(acrylic acid), the values of the surface areas were averaged for the three isotherms to determine V_{mon} and a value for c was calculated using eq 2 for each of the temperatures used in the NMR experiments taking ΔH_{ads} to be 4.2 kcal/mol. Knowing p_0 from saturated vapor pressure measurements,[23] eq 1 was used to calculate the coverage θ, which is equal to V/V_{mon}. We could therefore estimate the xenon coverages relatively accurately without having to do an isotherm at each of the experimental temperatures by assuming ΔH_{ads} to be constant.

III. Results

As in the case of zeolites, the line shape and chemical shift of adsorbed xenon is extremely sensitive to the presence of water on the polymer surface. The large affinity of poly(acrylic acid) for water is evident from the spectra shown in Figure 5 of xenon adsorbed onto samples which received different pretreatments. Figure 5b shows the spectrum of xenon adsorbed onto a sample that had been evacuated at room temperature for two hours. The line width is very large, over 100 ppm, indicating that the xenon experiences a variety of environments on the surface that are not averaged over the NMR time scale (~10^{-6} s). In contrast, a relatively narrow resonance is observed for a poly(acrylic acid) sample which had been heated under vacuum at 80 °C overnight. This treatment produces a much more homogeneous surface as evidenced by the xenon line shape. In Figure 5a, the chemical shift of xenon on the heat treated polymer is 136 ppm, which corresponds to the high-frequency edge of the broad resonance on the sample evacuated at room temperature. This distribution of lower chemical shifts probably results from a mediation of the xenon–surface interaction by the surface water. We have also observed that the xenon relaxation time is considerably shorter on the hydrated surface, which makes the experiment difficult to perform under equilibrium conditions. The increase in the xenon relaxation rates may be due to additional fluctuating proton–xenon dipolar interactions with mobile surface water. This

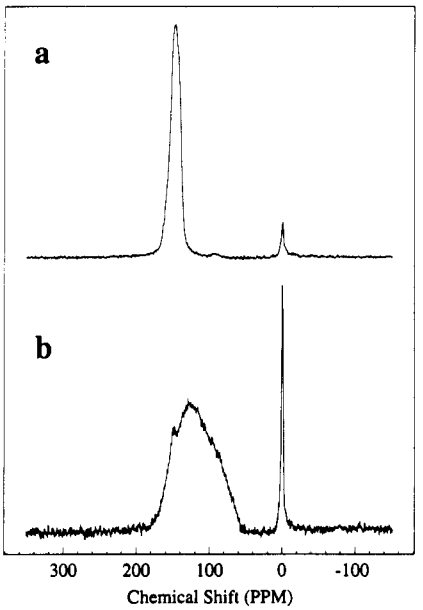

Figure 5. ^{129}Xe NMR spectra of xenon adsorbed at −140 °C onto poly(acrylic acid) that had been evacuated previously (a) overnight at 80 °C and (b) at room temperature for several hours.

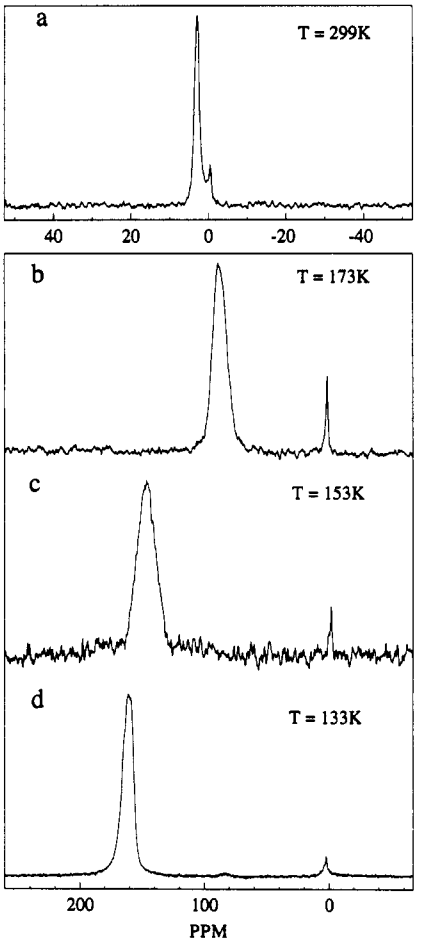

Figure 6. Representative ^{129}Xe NMR spectra of xenon adsorbed onto poly(acrylic acid) at various temperatures and pressures: (a) T = 299 K, P = 30 Torr; (b) T = 173 K, P = 20 Torr; (c) T = 153 K, P = 10 Torr; (d) T = 133 K, P = 2 Torr.

trend is in contrast to that of xenon adsorbed into NaY zeolite in which the relaxation rate is found to decrease with increasing water content.[24]

In Figure 6, the NMR spectra of optically pumped ^{129}Xe adsorbed onto poly(acrylic acid) at different temperatures show a peak at 0 ppm due to xenon gas and peaks at higher chemical

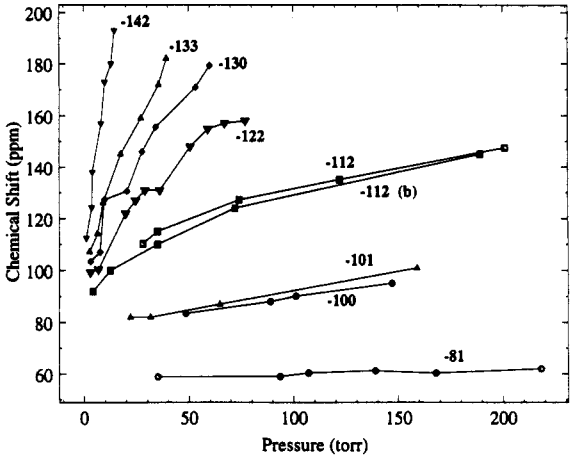

Figure 7. ^{129}Xe chemical shifts (ppm) of xenon adsorbed on poly(acrylic acid) as a function of pressure at the different equilibrium temperatures measured. The shifts are referenced to xenon gas at zero pressure. Lines connect the points at each temperature to guide the eye.

shifts due to adsorbed xenon. The spectra are quite different from those of an earlier study of xenon adsorbed on benzanthracene[18] in two ways. First, at room temperature, there is already a distinct peak at 3 ppm for adsorbed xenon which is not observed in the case of benzanthracene.[18] This is due both to the higher surface area of the poly(acrylic acid) (~15 m^2/g) over that of benzanthracene (~0.5 m^2/g), which increases the probability of finding xenon at the surface, and to a stronger xenon–surface interaction as manifested by the larger chemical shifts observed on poly(acrylic acid) at low temperatures. Second, the line widths of the spectra are narrower than for xenon on benzanthracene, due either to a higher surface mobility or to a more homogeneous surface.

The full data set for the chemical shift of xenon adsorbed on poly(acrylic acid) is given in Figure 7 as a function of temperature and pressure. As the temperature is lowered, the chemical shift of the adsorbed xenon increases fairly rapidly. The variation of the pressure dependence of the adsorbed xenon shift with temperature is even more pronounced, as seen by the sharp increase of the chemical shift slopes at the lower temperatures.

IV. Discussion

The large temperature and pressure dependence of the adsorbed xenon can be understood in terms of the xenon sticking time and diffusion on the polymer surface. Since the gas peak does not shift appreciably with temperature, the two observed resonances do not represent xenon simply exchanging between a pure gas phase and an adsorbed phase. Instead, the xenon resonances reflect the two different regions which are present in the sample volume. First, there is the relatively isolated xenon in the gas phase with a chemical shift of 0 ppm. At room temperature, this is a sizable fraction of the xenon, but as the temperature is lowered, this fraction diminishes until about 130 K where the gas signal is no longer observed. The other fraction of xenon is in contact with the sample and is rapidly exchanging between the gas phase and the surface-adsorbed phase so that its chemical shift reflects an averaging of the xenon over the different environments.

The chemical shift of dilute xenon gas is given[25] by a virial-type expansion:

$$\delta(T,\rho) = \sigma_0(T) + \sigma_1(T)\rho + \sigma_2(T)\rho^2 + \ldots \quad (3)$$

where the $\sigma(T)$ are the virial coefficients of the nuclear shielding. Likewise, the chemical shift of xenon in contact with the polymer surface can be written in terms of a pure Xe–surface term $\sigma_{os}(T)$ and a *surface* xenon–xenon interaction, $\sigma_{1s}(T)$:

$$\delta(T,\theta) = P_s\sigma_{os}(T) + (P_s)^2\sigma_{1s}(T)\theta + (P_s)^3\sigma_{2s}(T)\theta^2 + \ldots \quad (4)$$

where P_s is the probability of finding xenon at the surface and

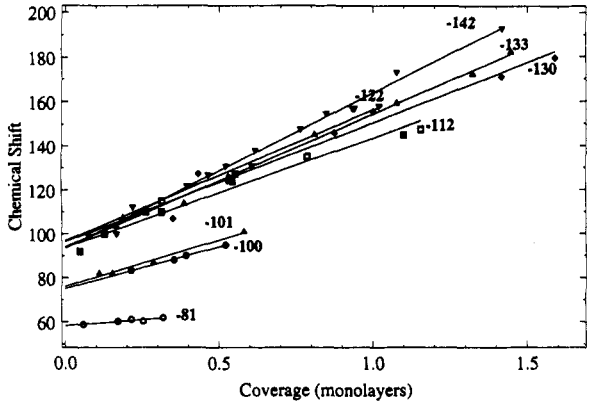

Figure 8. ^{129}Xe chemical shifts (ppm) as a function of the equilibrium temperature and coverage (in monolayers). Lines represent linear least-squares fits to the data at each temperature.

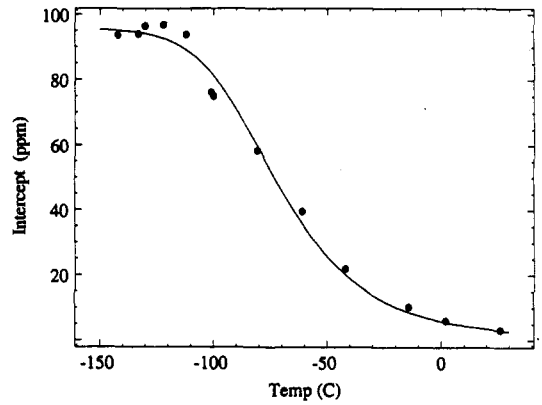

Figure 9. ^{129}Xe chemical shift intercepts, δ_s (ppm) versus temperature. The solid line is the fit to the data using eq 9 described in the text.

θ is the coverage in monolayers. The $(P_s)^2\sigma_{1s}\theta$ term is due to the xenon–xenon collisions which occur at or near the surface and gives rise to the observed slope of the chemical shift as a function of pressure or coverage. Fraissard has shown that the large adsorption energy in zeolites leads to an effective pressure of xenon that is quite high, resulting in many xenon–xenon collisions[26] and observes a linear dependence of chemical shift on pressure in NaX zeolite. In our experiments the xenon chemical shift on poly(acrylic acid) also appears to be a *linear* function of the pressure at all temperatures. Therefore only the binary collisions appear to be important at the xenon coverages studied and the σ_{2s} and higher order terms can be neglected. In addition, the pressure dependence of the xenon chemical shift on poly(acrylic acid) increases dramatically at lower temperatures.

To analyze the latter effect, xenon isotherms were used to convert the temperature and pressure data to xenon coverages. The chemical shift as a function of the coverage, θ, covers a range from 0.03 monolayers to about 1.5 monolayers of xenon on the polymer surface and is displayed in Figure 8. The chemical shift is found to be a linear function of coverage, although the slopes increase more modestly than the pressure dependent plot. The range from about 11 ppm/monolayer at −81 °C, to about 70 ppm/monolayer at −142 °C. The slopes and intercepts of the data in Figure 8 can be analyzed in terms of a surface residence probability and the xenon–xenon chemical shift temperature dependence, as derived by Jameson and co-workers[25] and extrapolated to our experimental conditions.

The chemical shift intercepts of the adsorbed xenon resonances (that is, excluding xenon–xenon interactions) can be modeled as a chemical exchange problem such that the chemical shift consists of surface and gas (δ_g) contributions, which are weighed by the probabilities, P_s and P_g, of finding xenon in each phase:

$$\delta = \sigma_{os}P_s + \delta_g P_g \tag{5}$$

where $P_s + P_g = 1$. However, δ_g is our reference defined to be zero, so

$$\delta = \sigma_{os}P_s \tag{6}$$

The probability of finding a xenon atom at the surface is given by

$$P_s = \tau_s/(\tau_s + \tau_\nu) \tag{7}$$

where τ_s is the sticking time, and τ_ν is the reciprocal of the collision rate with the surface. The average sticking time at the surface is given by

$$\tau_s = \tau_0 e^{\Delta H_{ads}/kT} \tag{8}$$

where τ_0 is the preexponential factor which we take to be 10^{-12} s[27] and ΔH_{ads} is the energy of adsorption. Using the adsorption energy calculated from the xenon isotherms, 4.2 kcal/mol, we find that the sticking times range from $\sim 10^{-9}$ s at room temperature to 10^{-5} s at 130 K. The chemical shift extrapolated to zero pressure can thus be fit to a function of the form of eq 6 where P_s is given by

$$P_s = \frac{\tau_0 e^{\Delta H_{ads}/kT}}{\tau_\nu + \tau_0 e^{\Delta H_{ads}/kT}} \tag{9}$$

by substituting eq 8 into eq 7. Although it is not possible to separate the variables τ_0 and τ_ν in the fit, with $\Delta H_{ads} = 4.2$ kcal/mol and choosing $\tau_0 = 10^{-12}$, we find that $\delta_s = 95$ ppm and $\tau_\nu = 3 \times 10^{-8}$ s. The chemical shift intercept data fitted to eq 9 are given in Figure 9. The contribution to the chemical shift due to the xenon–surface interaction is therefore 95 ppm, a value somewhat larger than 86 ppm measured for xenon in NaY zeolite at 144 K.[28] In view of the much smaller heat of adsorption of xenon on the polymer as compared to a zeolite, this large value for δ_s is surprising. However for NaY δ_s increases from 56 ppm at room temperature, to 86 ppm at 144 K, the only low temperature measured, so it may increase further at even lower temperatures. In addition, it is difficult to compare our results for the xenon/polymer system to the small body of low-temperature xenon shift data which has been measured for porous materials since the xenon shift is also highly sensitive to the morphology of the sample. Several studies have shown that a large value for δ_s on a sample with a small heat of adsorption can be due to the surface structure. For example, Cheung found that although the adsorption sites in amorphous silica–alumina mixtures[29] are much weaker than in NaY zeolite, the zero pressure xenon shifts are much larger, greater than 120 ppm at 144 K. This behavior may be due to a broad distribution of micropores in these amorphous samples and the fact that the ^{129}Xe chemical shift is inversely proportional to the pore size. Fraissard and co-workers obtained similarly large xenon shifts for a material consisting of agglomerated silica spheres[30] although the pores sizes are an order of magnitude larger than those in zeolites. In this case, the large chemical shifts are attributed to rapid exchange between the interporous xenon atoms and xenon adsorbed into confined spaces at the points of contact between the silica spheres. From the observed BET behavior of the xenon isotherms on poly(acrylic acid), we surmise that this amorphous polymer is not microporous like amorphous silica. Thus we believe that the chemical shift is due to xenon interacting with surface functional groups; however, we cannot completely rule out the possible existence of some type of surface microstructure responsible for the relatively large xenon shift at low coverages.

The ^{129}Xe NMR data also contains information about diffusion of xenon on the surface. This is extracted from the coverage dependence of the adsorbed xenon chemical shift which arises from the xenon–xenon interactions at the polymer surface as

given by the second term in the virial expansion (4). Taking the derivative of eq 4 gives

$$d\delta/d\theta = P_s^2\sigma_{1s}(T) \quad (10)$$

which is the slope of our chemical shift data (Figure 8). As an approximation, we can relate $\sigma_{1s}(T)$ to the second viral coefficient of the nuclear shielding, $\sigma_1(T)$, as defined by Jameson,[25] which determines the contribution to the gas-phase shift due to Xe–Xe collisions. For all gases, $\sigma_1(T)$ has been found to have the same sign since the gas-phase intermolecular interactions always result in a net deshielding of the nucleus. In xenon, however, this parameter is unusually large, ranging from 0.75 to 0.1665 ppm/amagat between 240 and 440 K. We must extrapolate these values down to our low temperatures range, to about 130 K. To relate the gas-phase Xe–Xe interactions to a surface interactions, we will assume that the nature of the pairwise collisions is not greatly changed by the presence of a surface. This of course is not strictly correct (in fact, the possibility of forming Xe–Xe bonds on a strongly adsorbing surface, palladium metal, has even been explored theoretically[31]), but it is reasonable to assume that a weakly adsorbing surface such as a polymer will not greatly perturb the xenon–xenon interactions. However, the contribution to the shift due to the xenon–xenon interactions also depends on the collision *rate*, which will be very different on a surface. In the gas phase, the collision rate is given by

$$1/\tau_c = [Xe]\sigma_{Xe}\bar{\nu}_g = \bar{\nu}_g^2/3D_g \quad (11)$$

where [Xe] is the xenon concentration, $\bar{\nu}_g$ is the average relative velocity, σ_{Xe} is the binary collision cross section (23 Å^2 for xenon), and D_g is the gas diffusion constant. The average relative velocity is $\bar{\nu}_g = (16kT/\pi m)^{1/2}$. On a surface, a similar expression is given for the collision rate:

$$1/\tau_{sc} = \theta\sigma_s\bar{\nu}_s = \bar{\nu}_s^2/2D_s \quad (12)$$

where θ is the coverage, D_s is the surface diffusion constant, $\bar{\nu}_s^2$ is the surface velocity, and the units of θ and σ_s are now cm^{-2} and cm. Since at monolayer coverages there will be two-dimensional diffusion on the surface, the constant is $^1/_2$ instead of $^1/_3$ in the expression for $1/\tau_{sc}$. With the assumption that the xenon–xenon interactions only differ due to the collision rates in the two phases, we scale the known gas-phase coefficient by the ratio of the two rates:

$$\sigma_{1s}(T) = \sigma_1(T)\tau_c/\tau_{sc} \quad (13)$$

The equation for the coverage dependence of the adsorbed xenon chemical shift can now be rewritten using eqs 11 and 12 for the collision rates:

$$d\delta/d\theta = P_s^2\sigma_{1s}(T) = P_s^2\sigma_1(T)2\theta^2\sigma_s^2D_s/[Xe]\sigma_{Xe}\bar{\nu}_g \quad (14)$$

The chemical shift slope data of Figure 8 can be fit to this expression in order to extract a value for the diffusion coefficient. The coverage, θ, on the right side of eq 14 is a constant and not a variable since $\sigma_1(T)$ is determined at a constant pressure. D_s will be evaluated at a coverage of 1 monolayer, so that $\theta = {}^1/_{23}$ Å^2. All of the parameters in eq 14 are known, with the exception of P_s, which is found from a fit to the chemical shift intercepts in Figure 9, and $\sigma_1(T)$, which is extrapolated from the gas-phase data in ref 25, and D_s, which we would like to determine.

The xenon chemical shift slopes fit to eq 14 are presented in Figure 10. Although there is some scatter, it is apparent that a simple linear fit would be inadequate to describe the data. The pressure dependence should tend to zero at the higher temperatures where the xenon spends little time at the polymer surface and the slope should be merely the room temperature value of the second viral coefficient, 0.548 ppm/amagat. By substituting in values for σ_s (8.8 Å) and θ ($^1/_{23}$ Å^2), the value of D_s is found to be 3.3 × 10^{-5} cm^2 s^{-1}.

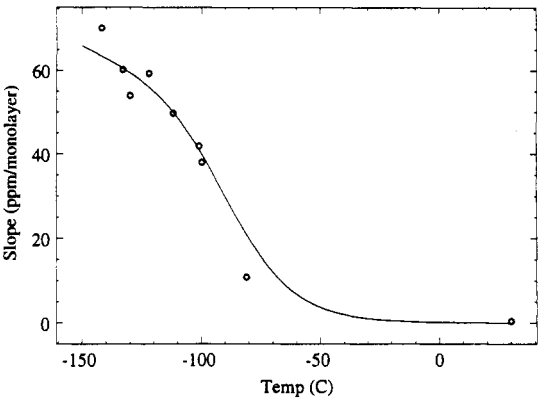

Figure 10. ^{129}Xe chemical shift slope (ppm/monolayer) versus temperature fitted to the data using eq 14.

By including a second parameter into the fit, an Arrhenius form,

$$D(T) = D_0e^{-E_{diff}/kT} \quad (15)$$

the temperature-dependent diffusion coefficient could be determined. However, the quality of the fits did not allow us to determine E_{diff}. This probably due both to the fact that there was already an exponential temperature dependence in the fit of the chemical shift slopes as well as an underestimate of the second viral coefficient of the nuclear shielding, at lower temperatures where we had to extrapolate the data of Jameson et al. more than 100 °C. In light of the small energy of adsorption for xenon on the polymer, however, the temperature dependence of the diffusion may be relatively small. In general E_{diff} is expected to be 10–20% of the adsorption energy,[27] which is 4.2 kcal/mol for xenon on poly(acrylic acid) and would lead to a decrease of the diffusion constant only by a factor of 2 over the temperature range studied. It is also worth noting that the value of D_s we calculate from our method is comparable to the diffusion coefficients of methane and neopentane on graphitized carbon measured by pulsed linear field gradient methods. For example, at a coverage of one monolayer at 85 K, $D_s = (5 \pm 2) \times 10^{-5}$ cm^2/s for methane on graphitized carbon black and $D_s = (3.0 \pm 0.5) \times 10^{-5}$ cm^2/s at 228 K for neopentane at a coverage of 1.25 monolayer on the same substrate.[32]

V. Conclusions

In this paper we report the first NMR study of xenon adsorbed onto the surface of a polymer. We have polarized xenon gas by optical pumping and measured the chemical shifts of xenon adsorbed onto poly(acrylic acid) as a function of temperature and pressure. The dynamical parameters extracted from our analysis of the chemical shift behavior of xenon in contact with poly(acrylic acid) indicate that the xenon is still highly mobile on the polymer surface at the lowest temperatures measured. The diffusion constant estimated for xenon on poly(acrylic acid) is similar to that of small molecules on graphite. From the value of the diffusion coefficient and assuming Fick's law, the translational correlation time τ_t is of the order $\sim 10^{-10}$ s. Since the efficiency of cross polarization deteriorates with increasing molecular motion, our data indicate that lower temperatures will be necessary before cross polarization experiments between the polarized xenon and the surface spins can be attempted. In a theoretical study of the effect of molecular motion on ^{1}H–^{13}C cross polarization, Schulze et al.[33] found that the efficiency of magnetization transfer decreases dramatically for motional correlation times shorter than $\sim 10^{-5}$ s. In addition to the dynamical data, the chemical shift extrapolated to zero coverage indicates a surprisingly strong interaction between xenon and poly(acrylic acid), which may be due to the polar carboxylic acid functional groups at the polymer surface. These chemical shifts

are less than those observed for xenon occluded into polymers such as polyethylene (198 ppm)[34] or in polymer blends (192–215 ppm).[35] We are currently investigating the source of this interaction by measuring the spin-polarized xenon chemical shifts on a homologous series of polymer surfaces.

Acknowledgment. This work was supported by the Director, Office of Energy Research, Office of Basic Energy Sciences, Materials Sciences Division, U.S. Department of Energy under Contract No. DE-AC0376SF0098. P.T. gratefully acknowledges support from IBM. H.L. thanks Chevron for a fellowship.

References and Notes

(1) Fyfe, C. A. *Solid State NMR for Chemists*; CFC Press: Guelph, Ontario, 1983.

(2) Gonen, O.; Kuhns, P. L.; Waugh, J. S.; Fraissard, J. P. *J. Am. Chem. Soc.* **1989**, *23*, 504.

(3) Pines, A.; Gibby, M. G.; Waugh, J. S. *J. Phys. Chem.* **1973**, *59*, 569.

(4) (a) Kastler, A. *J. Phys. Radium* **1950**, *11*, 255. (b) Bernheim, R. A. *Optical Pumping: An Introduction*; Benjamin: New York, 1965.

(5) Happer, W. *Rev. Mod. Phys.* **1972**, *44*, 169.

(6) (a) Grover, B. C. *Phys. Rev. Lett.* **1978**, *40*, 391. (b) Baskar, N. D.; Happer, W. *Phys. Rev. Lett.* **1982**, *49*, 25. (c) Kwon, T. M.; Mark, J. G.; Volk, C. H. *Phys. Rev. A* **1981**, *24*, 1894.

(7) (a) Wu, Z.; Happer, W.; Daniels, J. M. *Phys. Rev. Lett.* **1987**, *59*, 1480. (b) Wu, Z.; Happer, W.; Kitano, M.; Daniels, J. M. *Phys. Rev. A* **1990**, *42*, 2774. (c) LeFevre-Seguin, V.; Brossel, J. *J. Low Temp. Phys.* **1988**, *72*, 165.

(8) Cates, G. D.; Benton, D. R.; Gatzke, M.; Happer, W.; Hasson, K. C.; Newbury, N. R. *Phys. Rev. Lett.* **1990**, *65*, 2591.

(9) (a) Springuel-Huet, M. A.; Fraissard, J. *Chem. Phys. Lett.* **1989**, *154*, 299. (b) Ito, T.; Fraissard, J. *Zeolites* **1988**, *8*, 350. (c) Davis, M. E.; Saldarriaga, C.; Montes, C.; Hanson, B. *J. Chem. Phys.* **1988**, *92*, 2557.

(10) Chmelka, B. F.; de Menorval, L. C.; Csencsits, R.; Ryoo, R.; Liu, S.-B.; Radke, C. J.; Petersen, E. E.; Pines, A. In *Structure and Reactivity of Surfaces*; Morterra, C., et al., Eds.; Elsevier: Amsterdam, 1989; p 269.

(11) (a) de Menorval, L. C.; Raftery, D.; Liu, S.-B.; Takegoshi, K.; Ryoo, R.; Pines, A. *J. Phys. Chem.* **1990**, *94*, 27. (b) Chmelka, B. F.; Pearson, J. G.; Liu, S.-B.; Ryoo, R.; de Menorval, L. C.; Pines, A. *J. Phys. Chem.* **1991**, *95*, 303.

(12) Ripmeester, J. A.; Ratcliffe, C. I.; Tse, J. S. *J. Chem. Soc., Faraday Trans. 1* **1988**, *84*, 3731.

(13) Fetter, G.; Tichit, D.; de Menorval, L. C.; Figueras, F. *Appl. Catal.* **1990**, *65*, L1.

(14) (a) Stengle, T. R.; Williamson, K. L. *Macromolecules* **1987**, *20*, 1428. (b) Kennedy, G. *J. Polym. Bull.* **1990**, *23*, 605.

(15) (a) Miller, K. W.; Reo, N. V.; Schoot Uiterkamp, A. J. M.; Stengle, D. P.; Stengle, T. R.; Williamson, K. L. *Proc. Natl. Acad. Sci. U.S.A.* **1981**, *79*, 4946. (b) Tilton, Jr., R. F.; Kuntz, I. D. *Biochemistry* **1982**, *21*, 6850.

(16) Slichter, C. P. *Annu. Rev. Phys. Chem.* **1986**, *37*, 25.

(17) (a) Chmelka, B. F.; Raftery, D.; McCormick, A. V.; de Menorval, L. C.; Levine, R. D.; Pines, A. *Phys. Rev. Lett.* **1991**, *66*, 580. (b) Jameson, C. J.; Jameson, A. K.; Gerald II, R.; De Dios, A. C. *J. Chem. Phys.* **1992**, *96*, 1676. (c) Jameson, C. J.; Jameson, A. K. *J. Chem. Phys.* **1992**, *96*, 1690.

(18) Raftery, D.; Long, H.; Meersmann, T.; Grandinetti, P. J.; Reven, L.; Pines, A. *Phys. Rev. Lett.* **1991**, *66*, 584.

(19) Raftery, D.; Long, H.; Reven, L.; Tang, P.; Pines, A. *Chem. Phys. Lett.* **1992**, *191*, 385.

(20) Baskar, N. D.; Happer, W.; Larsson, M.; Zeng, X. *Phys. Rev. Lett.* **1983**, *50*, 105.

(21) Doty, F. D.; Inners, R. R.; Ellis, P. *J. Magn. Reson.* **1981**, *43*, 399.

(22) Brunaver, S.; Emmett, P. H.; Teller, E. *J. Am. Chem. Soc.* **1938**, *60*, 309.

(23) (a) Freeman, M. P.; Halsley, Jr., G. D. *J. Phys. Chem.* **1956**, *60*, 1119. (b) Cook, G. A. *Argon, Helium and the Rare Gases*; Interscience: New York, 1961; Vol. 1.

(24) Smith, M. L.; Dybowski, C. *J. Phys. Chem.* **1991**, *95*, 4942.

(25) Jameson, C. J.; Jameson, A. K.; Cohen, S. M. *J. Phys. Chem.* **1973**, *59*, 4540.

(26) Ito, T.; Fraissard, J. *J. Phys. Chem.* **1982**, *76*, 5225.

(27) Somorjai, G. A. *Chemistry in Two Dimensions: Surfaces*; Cornell University Press: Ithaca, NY, 1981.

(28) Cheung, T. T. P.; Fu, C. M.; Wharry, S. *J. Phys. Chem.* **1988**, *92*, 5170.

(29) Cheung, T. T. P. *J. Phys. Chem.* **1989**, *93*, 7549.

(30) Conner, W. C.; Weist, E. L.; Ito, T.; Fraissard, J. *J. Phys. Chem.* **1989**, *93*, 4138.

(31) Hoffmann, R.; Kersting, M.; Nomikou, Z. *J. Phys. Chem.* **1991**, *95*, 4033.

(32) Tabony, J.; Cosgrove, T. *Chem. Phys. Lett.* **1979**, *67*, 103.

(33) Schulze, D.; Ernst, H.; Fenzke, D.; Meiler, W.; Pfeifer, H. *J. Phys. Chem.* **1990**, *94*, 3499.

(34) Stengle, T. R.; Williamson, K. L. *Macromolecules* **1987**, *20*, 1430.

(35) Walton, J. H.; Miller, J. B.; Roland, C. M. *J. Polym. Sci. B.* **1992**, *30*, 527.